Nonlinear intersubband terahertz absorption in asymmetric quantum well structures

M. Bedoya* and A. S. Camacho†
Physics Department, Universidad de los Andes, Bogotá, Colombia
(Received 27 April 2005; revised manuscript received 28 June 2005; published 21 October 2005)

The THz nonlinear absorption of asymmetric double quantum wells is calculated. The dependence of the absorption on different parameters of the quantum wells is studied. In particular, different values of the barrier and wells width are considered. Also, a dc field in the direction of growth of the wells is introduced in the calculations and the nonlinear absorption is obtained for different dc and ac field intensities. The nonlinear absorption is obtained by using a perturbation calculation of the nonlinear susceptibility up to the third order within a density matrix approach. The absorption spectra are studied near the anticrossing of the first two excited subbands. Special attention is given to the nonlinear peaks due to the intensities of both fields. In particular some interesting negative nonlinear peaks are found and their dependence on the intensities of the fields is discussed.

DOI: 10.1103/PhysRevB.72.155318 PACS number(s): 78.20.Ci

I. INTRODUCTION

Semiconductor devices are a very important source of electromagnetic (EM) waves in daily life applications. But in the THz region of the EM spectrum, that spans from 100 GHz to 10 THz, there is an scarcity of compact solid-state sources that operate at room temperature.[1] In present times there is a need for such devices as a relatively long list of applications has been envisioned for the THz range: chemical detection, astronomy, wireless communications, atmospheric sensing, dental, biological, and medical imaging[1,2] are among the possible applications for this region.

Recently THz laser devices have been reported,[2,3] following the quantum cascade lasers (QCLs),[4] but no efficient or fast terahertz detectors are yet available.[5,6] Also THz emitters based on intersubband transitions in simple and asymmetric quantum wells have been proposed.[7–9]

Asymmetric multiple quantum wells are suited to the design of THz devices because their energies can be tuned so that the intersubband transitions in the conduction band lie in the THz range. In addition to that, the value of these transitions can be tailored by changing the geometry of the well and also by introducing a dc electric field in the growth direction of the layers.

Although some proofs of quantum coupling in asymmetric double quantum wells (ADQWs), based on tunneling from single QWs[10,11] have appeared, a systematic study of the coupling between the three first excited subbands in an asymmetric double quantum well giving rise to nonlinear absorption spectra is still lacking.

We present a systematic study of the intersubband nonlinear absorption of ADQWs designed for the THz range. The dependence of the absorption on various parameters of the quantum wells is studied. In particular, different values of the barrier and wells widths are considered, which account for the geometrical coupling of the wells and the corresponding eigenfunctions of the system. Also, a dc field in the direction of growth of the wells is introduced in the calculations,[12,13] as a second interaction for the 2D electronic gas in each subband, and the nonlinear absorption is obtained for different dc and ac field intensities. The second and third nonlinearities are strongly dependent on the geometry and the electric field applied showing well defined ranges of the parameters, for which the nonlinear absorption could be used in device applications.

An exact method, based on Ref. 16, is used to nonperturbatively calculate the energies, wave functions, and dipole moments. The nonlinear absorption is obtained by using a perturbative calculation of the nonlinear susceptibility up to the third order within a density matrix approach. The intersubband linear and nonlinear absorption of an ADQW can be tuned using three parameters of design: the width of the barrier between the wells that controls the coupling, the width of the narrow well that controls the asymmetry in the structure, and the strength of the external dc field applied in the growth direction of the structure.

Special attention is given to the nonlinear peaks due to the intensities of both fields the dc field and the radiation ac field, which induces the nonlinear effects. We are only interested in the three lowest transitions in the asymmetric DQW device coming from the first and second subbands of the wide well and the ground state of the narrow well as function of the barrier width. In particular, in studying the anticrossing region, where the second subband of the wide well has almost the same energy as the ground state subband of the narrow well and therefore the strongest coupling between the two wells is reached. On the other hand, when the ADQW is used as a THz detector we found nonlinear gains (negative absorption) around 5 THz with very low radiation field intensity for thinner barriers and with dc fields up to 14 kV/cm. It is worth to note that the nonlinear peaks of the absorption spectra as function of the external electric field show a giant response when the third subband of the device lies just at the energy edge of the well almost independent of the intensity of the radiation. Such a feature shows the effect of an interaction with the extended states of the continuum. We present in Sec. II the theoretical model used and in Sec. III A the linear and nonlinear absorption results without electric field are discussed. In Sec. III B the effect of a dc field is shown. Then in Sec. III C the most striking features due to

the coupling of the two wells in an ADQW under strong dc field are presented.

II. THEORY

A. Transfer matrix method with Airy functions

The transfer matrix method (TMM) is used to calculate the eigenenergies and the eigenfunctions as in Refs. 14 and 15. When a dc electric field is applied in the growth direction of the quantum wells (z direction) the potential $V(z)$ is biased.[15]

The value of the potential is $V_i - eFz$ for the region $z_{i-1} \leqslant z \leqslant z_i$, where F is the intensity of the electric field. The effective mass Schrödinger equation for the ith region can be written as[16]

$$-\frac{\hbar^2}{2m_i}\frac{d^2}{dz^2}\varphi_i(z) + (V_i - eFz)\varphi_i(z) = E\varphi_i(z). \tag{1}$$

This equation corresponds to a one band model in the presence of a dc electric field and holds for GaAs/AlGaAs materials due to the large bandgap. Equation (1) can be transformed into the Airy differential equation introducing a convenient change of variable,[17] and its solution can be written in the following way:

$$\varphi_i(z) = C_i^+ A[\eta_i(z)] + C_i^- B[\eta_i(z)], \tag{2}$$

where $A(x)$ and $B(x)$ are the solutions of the Airy equation and $\eta_i(z)$ is a function of $V_i(z)$ and F:

$$\eta_i = -\left(\frac{2m_i}{(e\hbar F)^2}\right)^{1/3}(E - V_i - eFz). \tag{3}$$

As in TMM with exponentials we can use Eq. (2) and the boundary conditions [Eqs. (4) and (5)] to obtain the coefficients $C_i^{\pm}$ for the wave functions and the eigenenergies:

$$\varphi_i(z_i) = \varphi_{i+1}(z_i), \tag{4}$$

$$\frac{1}{m_i}\frac{d\varphi_i(z_i)}{dz} = \frac{1}{m_{i+1}}\frac{d\varphi_{i+1}(z_i)}{dz}. \tag{5}$$

B. Density matrix formalism

Formalism of quantum mechanics. For the nonlinear absorption calculation a perturbative solution of the density matrix is necessary.[18] The Hamiltonian $\hat{H}$ is decomposed in two parts, the unperturbed term $\hat{H}_0$ for one electron in the quantum well and a time dependent interaction potential $\hat{V}(t)$ representing the perturbation

$$\hat{H} = \hat{H}_0 + \hat{V}(t). \tag{6}$$

The density matrix is defined as

$$\rho = |\psi\rangle\langle\psi|. \tag{7}$$

Including some phenomenological damping terms the time evolution equation for the density matrix is

$$\dot{\rho}_{nm} = \frac{-i}{\hbar}[\hat{H}, \hat{\rho}]_{nm} - \gamma_{nm}(\rho_{nm} - \rho_{nm}^{\mathrm{eq}}), \tag{8}$$

where, $\dot{\rho}_{nm}$ is the nm element of $\dot{\rho}$, ρ_{nm}^{eq} is the equilibrium value of ρ_{nm}, and γ_{nm} is the decay rate of ρ_{nm}. The perturbation solution for Eq. (8) can be found in Ref. 18. For the nm element of order q of the density matrix, the following recursion equation is obtained:

$$\rho_{nm}^{(q)}(t) = \int_{-\infty}^{t} \frac{-i}{\hbar}[\hat{V}(t'), \hat{\rho}^{(q-1)}]_{nm} \times e^{(i\omega_{nm} - \gamma_{nm})(t'-t)}dt'. \tag{9}$$

C. Calculations of the susceptibility perturbation terms

1. Density matrix calculation of the linear susceptibility

For the calculation of the linear susceptibility the following perturbation term is used (dipole moment approximation):

$$\hat{V}(t') = -\hat{\mathbf{u}} \cdot \mathbf{E}(t'), \hat{\mathbf{u}} = e\hat{\mathbf{r}} \tag{10}$$

with the electric field represented as a wave superposition

$$\mathbf{E}(t) = \sum_p \mathbf{E}(\omega_p)e^{-i\omega_p t} \tag{11}$$

we obtain the first term of the perturbation expansion of the density matrix

$$\rho_{nm}^{(1)}(t) = \hbar^{-1}(\rho_{mm}^{(0)} - \rho_{nn}^{(0)})\sum_p \frac{\hat{\mathbf{u}}_{nm} \cdot \mathbf{E}(\omega_p)e^{-i\omega_p t}}{(\omega_{nm} - \omega_p) - i\gamma_{nm}}. \tag{12}$$

Now we can calculate the expectation value for the dipole moment

$$\langle \mathbf{u}(t) \rangle = \mathrm{tr}(\hat{\rho}^{(1)}\hat{\mathbf{u}}) = \sum_{nm} \rho_{nm}^{(1)}\mathbf{u}_{mn}. \tag{13}$$

$\langle \mathbf{u}(t) \rangle$ can be expressed as a sum of frequency components

$$\langle \mathbf{u}(t) \rangle = \sum_p \langle \mathbf{u}(\omega_p) \rangle e^{-i\omega_p t} \tag{14}$$

and the linear susceptibility is related to the polarization by the following equation:

$$\mathbf{P}^{(1)}(\omega_p) = N\langle \mathbf{u}(\omega_p) \rangle = \chi^{(1)}(\omega_p)\mathbf{E}(\omega_p), \tag{15}$$

where N denotes the atomic number density, that is the number of two-level atoms per unit volume. N does not depend on position. Following Eqs. (13)–(15) and integrating over all components ω_p of the electric field we obtain the susceptibility tensor

$$\chi_{ij}^{(1)}(\omega_p) = \frac{N}{\hbar}\sum_{nm} (\rho_{mm}^{(0)} - \rho_{nn}^{(0)})\frac{u_{mn}^i u_{nm}^j}{(\omega_{nm} - \omega_p) - i\gamma_{nm}}. \tag{16}$$

2. Second and third order susceptibilities

The second order term of the density matrix is [see Eq. (9)]

$$\rho_{nm}^{(2)}(t) = e^{-(i\omega_{nm}-\gamma_{nm})t}\int_{-\infty}^{t} dt' \frac{-i}{\hbar}[\hat{V}(t'),\hat{\rho}^{(1)}]_{nm} \times e^{(i\omega_{nm}-\gamma_{nm})t'}. \tag{17}$$

The following expression relates the second order polarization to the second order susceptibility tensor:

$$\mathbf{P}^{(2)}(\omega_p+\omega_q) = \sum_{jk}\sum_{(pq)} \chi_{ijk}^{(2)}(\omega_p+\omega_q,\omega_p,\omega_q) \times E_j(\omega_q)E_k(\omega_p) \tag{18}$$

then the susceptibility tensor for the one-dimensional case ($\chi_{zzz}^{(2)}$) is[18]

$$\chi^{(2)}(\omega_p+\omega_q,\omega_p,\omega_q) = \frac{N}{2\hbar^2}\sum_{lmn}(\rho_{ll}^{(0)}-\rho_{mm}^{(0)})u_{ln}u_{nm}u_{ml} \times\left\{\frac{1}{[(\omega_{nl}-\omega_p-\omega_q)-i\gamma_{nl}][(\omega_{ml}-\omega_p)-i\gamma_{ml}]} + \frac{1}{[(\omega_{nl}-\omega_p-\omega_q)-i\gamma_{nl}][(\omega_{ml}-\omega_q)-i\gamma_{ml}]} + \frac{1}{[(\omega_{nm}+\omega_p+\omega_q)+i\gamma_{nm}][(\omega_{ml}-\omega_p)-i\gamma_{ml}]} + \frac{1}{[(\omega_{nm}+\omega_p+\omega_q)+i\gamma_{nm}][(\omega_{ml}-\omega_q)-i\gamma_{ml}]}\right\}. \tag{19}$$

The calculation of the third order susceptibility is done with the same procedure of the second order susceptibility calculation. The result for the third order susceptibility (omitting the tensor indexes since we work in 1D) is[18]

$$\chi^{(3)}(\omega_p+\omega_q+\omega_r,\omega_p,\omega_q,\omega_r) = \frac{N}{\hbar^3}\mathcal{P}_{\mathcal{I}}\sum_{\nu nml}(\rho_{ll}^{(0)}-\rho_{mm}^{(0)})u_{ln}u_{n\nu}u_{\nu m}u_{ml} \times\left\{\frac{1}{[(\omega_{nl}-\omega_p-\omega_q-\omega_r)-i\gamma_{nl}][(\omega_{\nu l}-\omega_p-\omega_q)-i\gamma_{\nu l}][(\omega_{ml}-\omega_p)-i\gamma_{ml}]} + \frac{1}{[(\omega_{n\nu}+\omega_p+\omega_q+\omega_r)+i\gamma_{n\nu}][(\omega_{mn}-\omega_p-\omega_q)-i\gamma_{mn}][(\omega_{ml}-\omega_p)-i\gamma_{ml}]} + \frac{1}{[(\omega_{n\nu}+\omega_p+\omega_q+\omega_r)+i\gamma_{n\nu}][(\omega_{\nu l}-\omega_p-\omega_q)-i\gamma_{\nu l}][(\omega_{ml}-\omega_p)-i\gamma_{ml}]} + \frac{1}{[(\omega_{m\nu}-\omega_p-\omega_q-\omega_r)-i\gamma_{m\nu}][(\omega_{mn}-\omega_p-\omega_q)-i\gamma_{mn}][(\omega_{nl}-\omega_p)-i\gamma_{ml}]}\right\}, \tag{20}$$

where the $\mathcal{P}_{\mathcal{I}}$ term is the permutation operator. This means that the sum between brackets has to be made over all the permutations of the ω_p, ω_q, and ω_r terms.

D. Optical absorption coefficient

The absorption coefficient in a crystal can be expressed as a function of the electric susceptibility

$$\alpha(\omega) = 2\pi\frac{\omega}{n_r c\epsilon_0}\,\mathrm{Im}[\chi(\omega)], \tag{21}$$

where χ can be expressed as

$$\chi(\omega) = \chi_{zz}^{(1)}(\omega) + \chi_{zzz}^{(2)}(\omega)E_z(t) + \chi_{zzzz}^{(3)}(\omega)E_z^2(t) \tag{22}$$

we obtain the linear absorption using Eqs. (16) and (21),[21] it can be written[10,21]

$$\alpha(\omega) = \pi\frac{\omega}{n_r c\epsilon_0}\,\mathrm{Im}\left(\frac{N}{\hbar}\sum_{nm}(\rho_{mm}^{(0)}-\rho_{nn}^{(0)})\frac{u_{mn}u_{nm}}{(\omega_{nm}-\omega_p)-i\gamma_{nm}}\right), \tag{23}$$

TABLE I. Ranges for the parameters (Ref. 26).

W_1	10 nm
W_2	1–5 nm
B	2, 6, and 10 nm
F	0–32 kV/cm

$$\alpha(\omega) = \frac{\omega}{n_r c \epsilon_0} \frac{m_e K_B T}{\hbar^3 L_z} \sum_{nm} |u_{mn}|^2 \frac{\gamma_{nm}}{(\omega_{nm} - \omega_p)^2 + \gamma_{nm}^2} \times \ln\left(\frac{1 + e^{[(E_F - E_m)/K_B T]}}{1 + e^{[(E_F - E_n)/K_B T]}} \right). \quad (24)$$

The nonlinear absorption is calculated in a similar way.

III. RESULTS

We study the intersubband linear and nonlinear absorption spectra in an ADQW as a function of the barrier width between the wells, which is chosen as the coupling parameter of the system. The absorption spectra are obtained as function of the radiation field intensity. Additionally, we study the effect of an external dc electric field, which can also play the role of coupling parameter of the system. We discuss the changes in the linear and nonlinear absorption.

We present the results by following the absorption dependence on (1) W_2, the narrow well width, (2) B, the barrier width, and (3) F, the strength of the dc field (see Table I). The following parameters are common to all the quantum wells: GaAs is assumed for the wells and $Al_{0.2}Ga_{0.8}As$ for the barriers. A scheme of the ADQW used for the calculations is in Fig. 1.

A. Results without electric field

The linear absorption spectrum as a function of the narrow well width for a barrier of $B=20$ Å, as a strong coupled device, is presented in Fig. 2. We observe the anticrossing effect, which is a clear signature of a tunable, coherent, coupled quantum system by means of geometry design. As the barrier-width narrows, the energy gap at the anticrossing increases. In Fig. 3 the logarithm of the anticrossing energy gap (E_{32}) as a function of the barrier width is shown in order to confirm the anticrossing behavior.

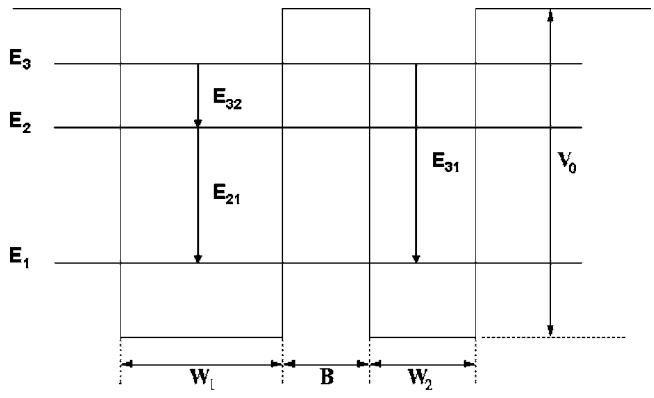

FIG. 1. Potential profile of an ADQW (Ref. 16).

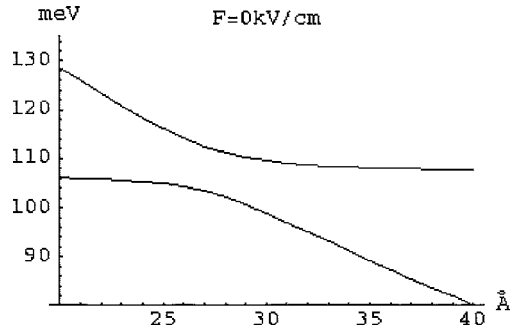

FIG. 2. Eigenenergies of the ADQW vs W_2 without external electric field for $B=60$ Å (Ref. 17).

In Fig. 4 the linear absorption as a function of the narrow well width for a barrier of $B=20$ Å is shown. The three peaks, observed at $W_2=20$ Å arising from the three possible transitions, shift in different directions as the narrow well width increases in the following way: the first one at 12 THz (E_{32}) is overcome by the second (E_{21}), initially at 17 THz, and starting from $W_2=35$ Å there is only one signal from both transitions with a maximum intensity. The third peak at 28 THz (E_{31}) suffers a redshift and its intensity is also increasing with W_2. This behavior can be understood in terms of the energy shifts due to geometry and as a signal of anticrossing.

When the coupling is weaker for a barrier of 60 Å (see Fig. 5), the linear absorption shows only one absorption peak corresponding to the transition E_{21} for W_2 thinner than 27 Å and to E_{31} for W_2 thicker than 28 Å, due to the anticrossing effect. Between 27 and 28 Å the peak is the sum of both transitions. The other two transition peaks are two orders of magnitude smaller than the value of the main peak and therefore are not observable. We notice that the geometric coupling affects severely the absorption spectrum of an ADQW for a barrier of $B=20$ Å, which corresponds to the strongest coupling. For this barrier the spectrum is richer than the one for $B=60$ Å. For the barrier of 100 Å the spectrum is very similar to the one for 60 Å with only one main absorption peak.

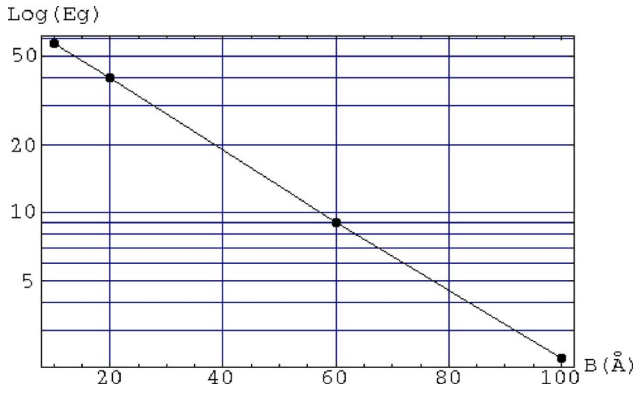

FIG. 3. (Color online) Energy gap vs B without external electric field (Ref. 18).

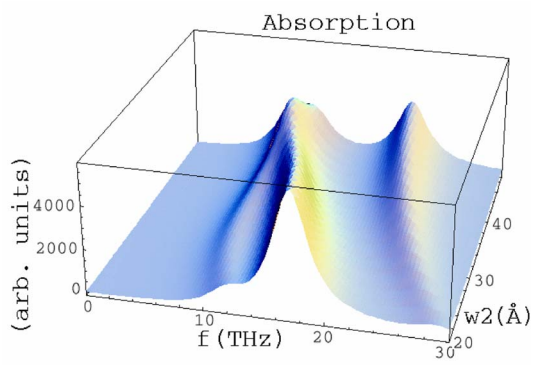

FIG. 4. (Color online) Linear absorption of the ADQW with $B=20$ Å vs W_2 without external electric field (Ref. 19).

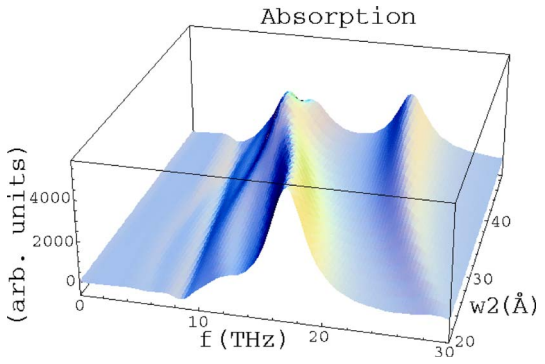

FIG. 6. (Color online) Nonlinear Absorption of the ADQW with $B=20$ Å vs W_2 with external radiation $E=5$ kV/cm (Ref. 21).

The intensity of the radiation ac field is another parameter that can be studied. We present the case of nonlinear absorption without external electric field in order to study the effect of the intensity of radiation on the absorption spectrum.

As we can see in Fig. 6, with a radiation field of 5 kV/cm, the nonlinear absorption spectrum for the case of strong coupling shows a new feature: the negative absorption at 8.5 THz, which also shifts to slightly lower energies as the narrow well width increases. It appears a gain due to the radiation field although its magnitude is small. This effect is due to the transition E_{21} and corresponds to a second order absorption. In this way we obtain gain in the THz region, below 10 THz.

B. Results with external electric field

Now, an external static electric field is introduced. Here we present the results for a fixed geometry varying only the electric field. An anticrossing also appears as a function of the field (F). In Fig. 7 the variation of the second and third eigenenergies with the electric field is shown for three different values of the barrier width. For the chosen parameters (Table II) the anticrossing lies at 14 kV/cm for $B=100$ Å, at 18 kV/cm for $B=60$ Å, and at 28 kV/cm for a barrier of 20 Å. It shifts to higher fields as the barrier width decreases, as a function of the geometrical coupling. The stronger the geometric coupling is, the higher the electric field to reach the maximum electric coupling. In Fig. 8 the logarithm of the anticrossing energy gap (E_{32}) is shown for several values of the electric field with $W_2=20$ Å. We observe that the electric field can be used as a suitable tuning parameter. It plays the same role as geometry regarding the coupling of the two wells. Figures 9(a) and 9(b) presents the nonlinear absorption vs W_2 for a barrier $B=20$ Å, an electric field of $F=4$ kV/cm and two weak intensities of the radiation ($E=0.1$ and 0.5 kV/cm).

When the radiation intensity is increased two new nonlinear peaks arise at 3.9 and 5.8 THz one corresponding to positive absorption and the other to negative absorption or gain. The main feature of these two peaks is that they appear only around $W_2=19$ Å, in this case at frequencies below 10 THz. These peaks correspond to the second and third order transition of $E_{32}(\simeq 12$ THz). Only very narrow wells, whose ground state is so high that it reaches the border of the quantum wells, show these two interesting peaks in the THz region. For thicker well widths the energy value decreases and therefore the absorption spectrum turns to be the expected one. This interesting nonlinear effect is to be explained through the sudden changing character of the eigenstate, which is a discrete state within the well and turns to be an extended state as it reaches the continuum.

The nonlinear absorption vs W_2 for a barrier $B=40$ Å [Figs. 9(c) and 9(d)], and the same dc electric field ($F=4$ kV/cm) shows two giant nonlinear peaks at intensities of

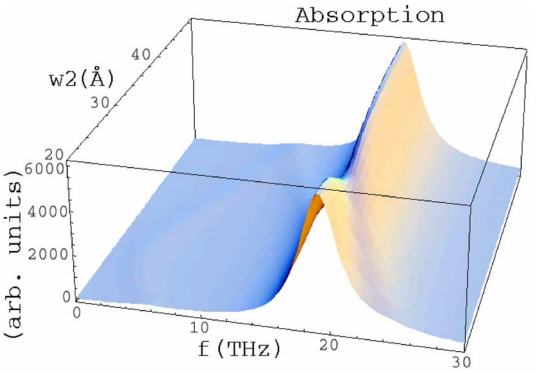

FIG. 5. (Color online) Absorption of the ADQW with $B=60$ Å vs W_2 without external electric field (Ref. 20).

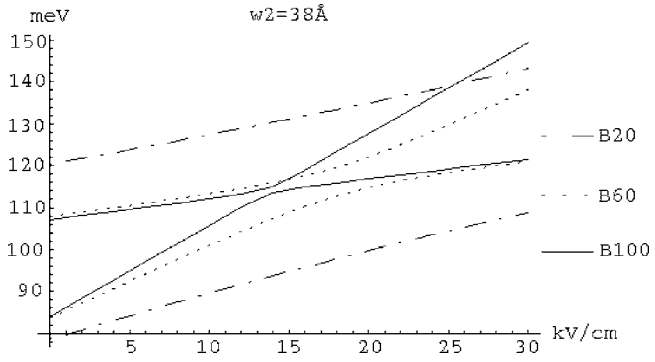

FIG. 7. Eigenenergies of the ADQW vs F without external electric field for $W_2=38$ Å (Ref. 22).

TABLE II. Parameters for all the cases (Ref. 27).

Effective mass for the wells	m_W	$0.0665m_0$
Effective mass for the barriers	m_B	$0.0832m_0$
Height of the barriers (or depth for the wells)	V_0	167 meV

the radiation field (E=3 kV/cm) higher than those required to obtain similar peaks for a barrier of B=20 Å. This is expected because the geometric coupling is weaker and therefore a starker intensity of the radiation field is needed. Only for the starker radiations fields is the nonlinear effect noticeable at very narrow wells. The linear peaks for this case are interpreted in the same way as in the case of B=20 Å. The first linear peak corresponds to E_{32}, the second to E_{21}, and the third to E_{31}; also an anticrossing effect is observed between E_{21} and E_{31}.

C. Nonlinear absorption as function of the electric dc field

In order to follow the nonlinear features observed at narrow wells, as function of the strength of the electric field, we calculate the absorption spectrum for several values of this parameter and we found that the giant nonlinear peaks move to wider well widths as the electric field increases, as expected. In Fig. 10 the absorption spectra for a barrier of 20 Å are presented for different values of the static electric field. We obtained new peaks around the old ones. For F =8 kV/cm their energies are 3.3 and 4.95 THz corresponding to the second and third nonlinear harmonics of E_{32} (W_2 =26 Å). For F=12 kV/cm their energies are 3.0 and 4.5 THz corresponding to the third and second nonlinear harmonics of E_{32}(W_2=36 Å). We identified all the peaks appearing in the spectra. The combined effect of the dc electric field

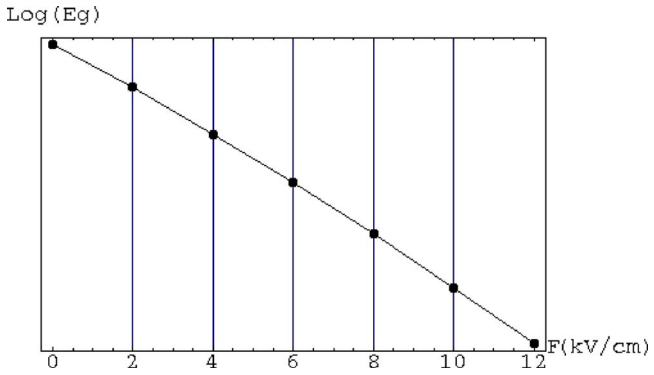

FIG. 8. (Color online) Energy gap vs F (Ref. 23).

and the radiation field will permit one to tune the wavelength at which the device works. At a very high electric field these anomalous nonlinear effects also affects the linear absorption peaks showing intensity changes for certain geometries. There are some values of W_2 at which the higher energy transition E_{31} is negligible and the nonlinear anomalies are giant. We conclude that both geometry and external field are important tuning parameters for intersubband-detectors and an adequate combination of both of them can bring an ideal tuning for device design.

D. Conclusions

Controlling intersubband transitions in quantum wells is important for device design based on these processes. In this work we present a study of the linear and nonlinear absorption as function of geometry and also as a function of an external dc field in the case of an ADQW of GaAs/AlGaAs. The two chosen coupling parameters have different physical meanings. The geometric parameters control the eigenenergies and eigenstates and an anticrossing is found, which appears for a geometric configuration of maximum coupling

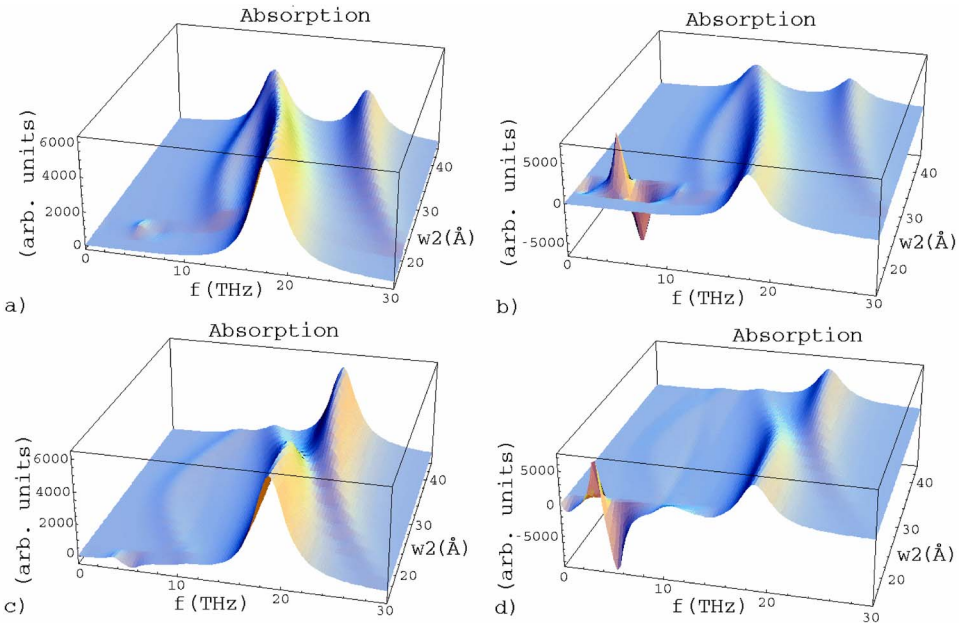

FIG. 9. (Color online) Nonlinear absorption vs W_2 with external electric field (F=4 kV/cm) for several barrier and radiation values (a) E=0.1 kV/cm, B=20 Å; (b) E=0.5 kV/cm, B=20 Å; (c) E=0.5 kV/cm, B=40 Å; and (d) E=3 kV/cm, B=40 Å (Ref. 24).

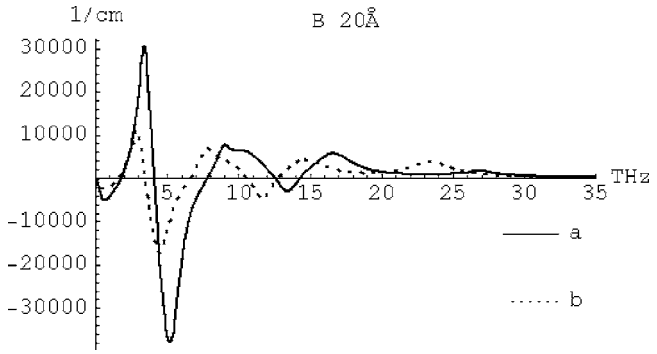

FIG. 10. Nonlinear absorption with $B=20$ Å for two cases (a) $F=8$ kV/cm, $E=0.5$ kV/cm and $W_2=26$ Å, (b) $F=12$ kV/cm, $E=1.0$ kV/cm, and $W_2=37$ Å (Ref. 26).

between the wells. The absorption spectra are strongly dependent on the coupling of the quantum wells; as it is shown for the strongest coupling the richness of absorption spectra is very useful for an application allowing us to tune with geometry the desired absorption peak. For weakly coupled systems the absorption spectra consist of only one peak and negligible anticrossing features were found.

An external dc field also couples the two wells in a similar way as geometry. We also found an anticrossing that depends on the field strength in this case. The electrical coupling serves as the tuner of the spectra and its effect is definitive because of the very new specific features appearing as the dc field is applied. When both coupling parameters are simultaneously examined we found that for very specific geometries, when the dc electric field is present, a giant effect appears due to the change of character of the third eigenenergy, which converts from a discrete state to a continuous state.

ACKNOWLEDGMENTS

The support by the Fondo de Investigaciones de la Facultad de Ciencias de la Universidad de los Andes and Colciencias Grant No. 1204–05–16852 is acknowledged.

*Electronic address: m-bedoya@uniandes.edu.co
†Electronic address: acamacho@uniandes.edu.co

[1] A. G. Davies, E. H. Linfield, and M. B. Johnston, Phys. Med. Biol. **47**, 3679 (2002).
[2] R. Köhler, A. Tredicucci, F. Beltram, H. E. Beere, E. H. Linfield, A. G. Davies, D. A. Ritchie, R. C. Iotti, and F. Rossi, Nature (London) **417**, 156 (2002).
[3] M. Rochat, L. Ajili, H. Willenberg, J. Faist, H. Beere, G. Davies, E. Linfield, and D. Ritchie, Appl. Phys. Lett. **81**, 1381 (2002).
[4] J. Faist, F. Capasso, D. L. Sivco, A. L. Hutchinson, C. Sirtori, and A. Y. Cho, Science **264**, 553 (1994).
[5] R. Köhler, R. C. Iotti, A. Tredicucci, and F. Rossi, Appl. Phys. Lett. **79**, 3920 (2001).
[6] C. Sirtori, Nature (London) **417**, 132 (2002).
[7] Benjamin S. Williams and Bin Xu, J. Appl. Phys. **90**, 5504 (2001).
[8] Benjamin S. Williams, Bin Xu, Quing Hu, and Michael R. Melloch, Appl. Phys. Lett. **75**, 2927 (1999).
[9] P. Kinsler, P. Harrison, and R. W. Kelsall, J. Appl. Phys. **85**, 23 (1999).
[10] E. Ozturk and I. Sokmen, J. Phys. D **36**, 2457 (2003).
[11] T. Matsusue, M. Tsuchiya, J. N. Schulman, and H. Sakaki, Phys. Rev. B **42**, 5719 (1990).
[12] J. N. Heyman, K. Craig, B. Galdrikian, M. S. Sherwin, K. Campman, P. F. Hopkins, S. Fafard, and A. C. Gossard, Phys. Rev. Lett. **72**, 2183 (1994).
[13] M. M. Fejer, J. J. B. Yoo, R. L. Byer, A. Harwit, and J. S. Harris, Jr., Phys. Rev. Lett. **62**, 1041 (1989).
[14] S. L. Chuang, *Physics of Optoelectronic Devices* (Wiley and Sons, New York, 1995).
[15] M. Luisier and S. Odermatt, Diploma thesis, ETH, Zurich, March, 2003.
[16] D. Ahn and S. L. Chuang, Phys. Rev. B **34**, 9034 (1986).
[17] D. A. B. Miller, D. S. Chemla, T. C. Damen, A. C. Gossard, W. Wiegmann, T. H. Wood, and C. A. Burrus, Phys. Rev. B **32**, 1043 (1985).
[18] R. W. Boyd, *Nonlinear Optics* (Academic Press, New York, 1992).
[19] P. Y. Han and X.-C. Zhang, Meas. Sci. Technol. **12**, 1747 (2001).
[20] M. Hangyo, T. Nagashima, and S. Nashima, Meas. Sci. Technol. **13**, 1727 (2002).
[21] D. Ahn and S. L. Chuang, IEEE J. Quantum Electron. **QE-23**, 2196 (1987).
[22] A. A. Batista, P. I. Tamborenea, B. Birnir, M. S. Sherwin, and D. S. Citrin, Phys. Rev. B **66**, 195325 (2002).
[23] Claire Gmachl, Alessandro Tredicucci, Deborah L. Sivco, Albert L. Hutchinson, Federico Capasso, and Alfred Y. Cho, Science **286**, 749 (1999).
[24] Carlo Sirtori, Federico Capasso, Deborah L. Sivco, and Alfred Y. Cho, Phys. Rev. Lett. **68**, 1010 (1992).
[25] E. Rosencher and P. Bois, Phys. Rev. B **44**, 11315 (1991).
[26] M. K. Gurnick and T. A. DeTemple, IEEE J. Quantum Electron. **19**, 791 (1983).
[27] P. F. Yuh and K. L. Wang, J. Appl. Phys. **65**, 4377 (1989).